REPORT DOCUMENTATION PAGE

Form Approved OMB NO. 0704-0188

The public reporting burden for this collection of information is estimated to average 1 hour per response, including the time for reviewing instructions, searching existing data sources, gathering and maintaining the data needed, and completing and reviewing the collection of information. Send comments regarding this burden estimate or any other aspect of this collection of information, including suggesstions for reducing this burden, to Washington Headquarters Services, Directorate for Information Operations and Reports, 1215 Jefferson Davis Highway, Suite 1204, Arlington VA, 22202-4302. Respondents should be aware that notwithstanding any other provision of law, no person shall be subject to any oenalty for failing to comply with a collection of information if it does not display a currently valid OMB control number.
PLEASE DO NOT RETURN YOUR FORM TO THE ABOVE ADDRESS.

1. REPORT DATE (DD-MM-YYYY)	2. REPORT TYPE	3. DATES COVERED (From - To)
	New Reprint	-

4. TITLE AND SUBTITLE	5a. CONTRACT NUMBER
Supramolecular Polymers with Orthogonal Functionality	W911NF-12-1-0339
	5b. GRANT NUMBER
	5c. PROGRAM ELEMENT NUMBER
	611102

6. AUTHORS	5d. PROJECT NUMBER
Souleymane Coulibaly, Christian Heinzmann, Frederick L. Beyer, Sandor Balog, Christoph Weder, Gina L. Fiore	
	5e. TASK NUMBER
	5f. WORK UNIT NUMBER

7. PERFORMING ORGANIZATION NAMES AND ADDRESSES	8. PERFORMING ORGANIZATION REPORT NUMBER
Case Western Reserve University 10900 Euclid Ave. Cleveland, OH 44106 -4919	

9. SPONSORING/MONITORING AGENCY NAME(S) AND ADDRESS (ES)	10. SPONSOR/MONITOR'S ACRONYM(S)
U.S. Army Research Office P.O. Box 12211 Research Triangle Park, NC 27709-2211	ARO
	11. SPONSOR/MONITOR'S REPORT NUMBER(S)
	62050-CH.6

12. DISTRIBUTION AVAILIBILITY STATEMENT

Approved for public release; distribution is unlimited.

13. SUPPLEMENTARY NOTES

The views, opinions and/or findings contained in this report are those of the author(s) and should not contrued as an official Department of the Army position, policy or decision, unless so designated by other documentation.

14. ABSTRACT

Supramolecular polymers with orthogonal interactions are of broad interest, and reports on such materials with multifunctional stimuli-responsive behavior are rare. Polymer blends based on a poly(ethylene-co-butylene) core (PEB) terminated with either 2-ureido-4[1H]-pyrimidinone (UPy) hydrogen-bonding motifs (UPy-PEB-UPy) or 2,6-bis(1?-methylbenzimidazolyl)pyridine (Mebip) ligands coordinated to metal ions ([M(Mebip-PEB-Mebip)]2+ (M = Zn, Fe)) were prepared. The degree of orthogonality of the supramolecular polymer blends was explored by UV?vis spectroscopy, small angle X-ray scattering, and dynamic mechanical thermal analysis (DMTA). Polymer

15. SUBJECT TERMS

metal-ligand coordination, hydrogen bonding, SAXS

16. SECURITY CLASSIFICATION OF:			17. LIMITATION OF ABSTRACT	15. NUMBER OF PAGES	19a. NAME OF RESPONSIBLE PERSON
a. REPORT	b. ABSTRACT	c. THIS PAGE			Stuart Rowan
UU	UU	UU	UU		19b. TELEPHONE NUMBER
					216-368-4242

Report Title

Supramolecular Polymers with Orthogonal Functionality

ABSTRACT

Supramolecular polymers with orthogonal interactions are of broad interest, and reports on such materials with multifunctional stimuli-responsive behavior are rare. Polymer blends based on a poly(ethylene-co-butylene) core (PEB) terminated with either 2-ureido-4[1H]-pyrimidinone (UPy) hydrogen-bonding motifs (UPy-PEB-UPy) or 2,6-bis(1?-methylbenzimidazolyl)pyridine (Mebip) ligands coordinated to metal ions ([M(Mebip-PEB-Mebip)]2+ (M = Zn, Fe)) were prepared. The degree of orthogonality of the supramolecular polymer blends was explored by UV?vis spectroscopy, small-angle X-ray scattering, and dynamic mechanical thermal analysis (DMTA). Polymer blends of [Zn(Mebip-PEB-Mebip)](NTf2)2 and UPy-PEB-UPy resulted in a statistical mixture of noncovalent interactions, whereas blends with [Fe(Mebip-PEBMebip)](ClO4)2 and UPy-PEB-UPy assembled in an orthogonal fashion. Additionally, the DMTA showed two transitions for the disassembly of UPy (ca. 60 °C) and Fe2+-Mebip (ca. 180 °C) phases. The Fe2+-Mebip interactions were selectively disrupted by the addition of a competitive ligand, demonstrating that each supramolecular motif can be targeted with either a thermal or chemical stimulus.

REPORT DOCUMENTATION PAGE (SF298)
(Continuation Sheet)

Continuation for Block 13

ARO Report Number   62050.6-CH
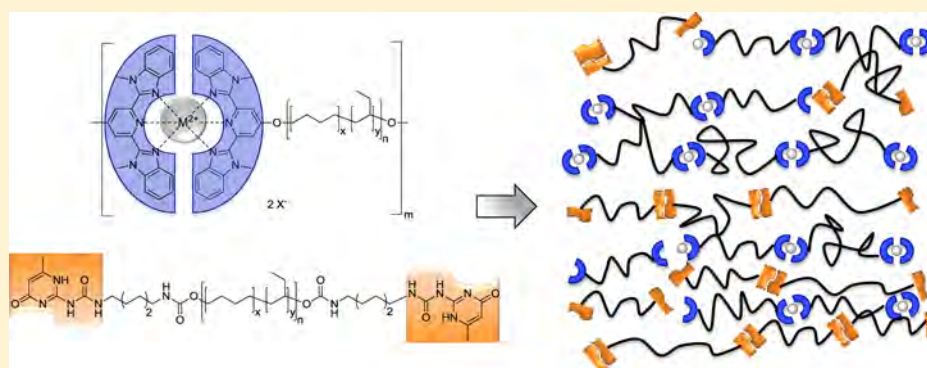Supramolecular Polymers with Orthogonal Func...

Supramolecular Polymers with Orthogonal Functionality

Souleymane Coulibaly,[†] Christian Heinzmann,[†] Frederick L. Beyer,[‡] Sandor Balog,[†] Christoph Weder,*,[†] and Gina L. Fiore*,[†]

[†]Adolphe Merkle Institute, University of Fribourg, Chemin des Verdiers 4, CH-1700 Fribourg, Switzerland

[‡]U.S. Army Research Laboratory, Aberdeen Proving Ground, Maryland 21005-5069, United States

S *Supporting Information*

ABSTRACT: Supramolecular polymers with orthogonal interactions are of broad interest, and reports on such materials with multifunctional stimuli-responsive behavior are rare. Polymer blends based on a poly(ethylene-*co*-butylene) core (PEB) terminated with either 2-ureido-4[1*H*]-pyrimidinone (UPy) hydrogen-bonding motifs (UPy-PEB-UPy) or 2,6-bis(1'-methylbenzimidazolyl)pyridine (Mebip) ligands coordinated to metal ions ([M(Mebip-PEB-Mebip)]$^{2+}$ (M = Zn, Fe)) were prepared. The degree of orthogonality of the supramolecular polymer blends was explored by UV−vis spectroscopy, small-angle X-ray scattering, and dynamic mechanical thermal analysis (DMTA). Polymer blends of [Zn(Mebip-PEB-Mebip)](NTf$_2$)$_2$ and UPy-PEB-UPy resulted in a statistical mixture of noncovalent interactions, whereas blends with [Fe(Mebip-PEB-Mebip)](ClO$_4$)$_2$ and UPy-PEB-UPy assembled in an orthogonal fashion. Additionally, the DMTA showed two transitions for the disassembly of UPy (ca. 60 °C) and Fe^{2+}-Mebip (ca. 180 °C) phases. The Fe^{2+}-Mebip interactions were selectively disrupted by the addition of a competitive ligand, demonstrating that each supramolecular motif can be targeted with either a thermal or chemical stimulus.

INTRODUCTION

Supramolecular polymers are of broad interest and offer several advantages over conventional polymers due to the dynamic nature of noncovalent interactions ($\pi-\pi$, metal−ligand, and hydrogen bonding). The latter serve to assemble the monomeric building blocks into polymeric structures and also enable controlled, reversible disassembly upon application of a specific stimulus, such as a change of temperature or pH, exposure to light, or the application of a mechanical force. This has allowed researchers to design a broad range of stimuli-responsive materials,[1] including thermally or optically healable polymers,[2−5] adhesives that permit bonding and debonding on demand,[6] chemically responsive mechanically adaptive nano-composites,[7] or magnetically addressable shape-memory materials.[8] The design of stimuli-responsive supramolecular polymers has largely focused on materials that contain one type of noncovalent interaction, which results in materials that respond to ideally one, but in many cases several, stimuli with a single response. Supramolecular polymers comprising different types of noncovalent binding motifs are rare,[9,10] but this design

could open up the door for the creation of multiresponsive polymers, i.e., materials that respond to different stimuli with different property changes. Weck et al.[11] recently reported a supramolecular ABC triblock copolymer that was assembled from heterotelechelic polymer core (B block) functionalized with a palladium−pincer complex and a hydrogen-bonding Hamilton receptor at the two termini and monofunctional A and C blocks that each carried one of the complementary binding motifs at one of their termini. ^{1}H NMR titration was used to demonstrate that the binding is indeed fully orthogonal, and selective and reversible dissociation of either the hydrogen-bonding or metal−ligand motifs was achieved by exposure to heat, the addition of a monotopic end-capping agent, or addition of triphenylphosphine.[12] However, these experiments were conducted in solutions, and no changes of solid-state properties were reported. Schubert et al. recently combined

metal-coordinate cross-links with terpyridine ligands and hydrogen-bonding UPy units to create supramolecular polymers, but due to the competitive coordination of the employed metal ions (Zn^{2+}, Ni^{2+}, Fe^{2+}) with UPy units, the binding of the supramolecular motifs was not completely orthogonal.[13,14] A supramolecular polymer with two orthogonal hydrogen-bonding motifs was reported by Meijer and Palmans et al.[15] Supramolecular assemblies with two types of hydrogen-bonding motifs were assembled as nanorods using benzene-1,3,5-tricarboxamide (BTA) and 2-ureido-4[1*H*]-pyrimidinone (UPy) based monomers. The mixture of these monofunctionalized nanorods resulted in a viscous liquid, and upon addition of a heterotelechelic building block containing both BTA and UPy motifs the viscous liquid transformed into a solid material with appreciable mechanical properties due to the formation of cross-links between the two populations. Thus, a few examples of supramolecular polymers with orthogonal binding motifs are emerging, but their potential multiresponsive behavior in the solid state has been little exploited.

Here, we report *blends* based on two supramolecular polymers based on an identical telechelic core, but different binding motifs at the termini, surmising that such materials could display multiresponsive behavior. The general design is based on the expectation that large-scale phase separation can potentially be avoided through the use of a common building block and that compositional variation over a large range is straightforward. We elected to utilize the widely employed poly(ethylene-*co*-butylene) (PEB) core[6,16−23] and decorated the latter with 2-ureido-4[1*H*]-pyrimidinone (UPy) motifs, which can dimerize in a self-complementary fashion, to create the hydrogen-bonded supramolecular polymer UPy-PEB-UPy,[6,19,23] and 2,6-bis(1′-methylbenzimidazolyl) pyridine (Mebip) ligands that can coordinate to metal salts (MX_2) and form metallosupramolecular polymers (MSPs) with the formula [M(Mebip-PEB-Mebip)](X)$_2$.[6,16,18,22] Using metal salts where M = Fe or Zn and X = ClO$_4$ or NTf$_2$, we prepared [Zn(Mebip-PEB-Mebip)](NTf$_2$)$_2$/(UPy-PEB-UPy) and [Fe-(Mebip-PEB-Mebip)](ClO$_4$)$_2$/(UPy-PEB-UPy) blends in which the ratio between the MSP and the hydrogen-bonded polymer was systematically varied. Through a systematic investigation of the composition−structure−property relationship, we demonstrate that in the case of the pair [Fe(Mebip-PEB-Mebip)](ClO$_4$)$_2$/(UPy-PEB-UPy) the binding is truly orthogonal and that certain characteristics of blends with appropriate composition can indeed be selectively altered by changing the assembly of either the metal−ligand or the hydrogen-bonding motifs by an external stimulus. The new material is one of the first examples of a supramolecular polymer system with orthogonal noncovalent binding motifs that displays multiple stimuli-responsive behavior in the solid state.

■ EXPERIMENTAL SECTION

Materials. UPy-PEB-UPy and Mebip-PEB-Mebip were synthesized from hydroxyl-terminated poly(ethylene-*co*-butylene) (M_n = 3100 g/mol, polydispersity index = 1.05), donated by Cray Valley SA (Krasol HLBH-P 3000), as previously reported.[6,18] Acidic impurities were removed from spectroscopic grade CHCl$_3$ by passage through a plug of dry, activated (Brockman I) basic alumina prior to use. Tetrahydrofuran was purified by passage through alumina columns.[24] Anhydrous CH$_3$CN (Sigma-Aldrich), chelidamic acid (Intatrade Chemicals GmbH), and all other solvents and reagents were used as received.

**Methods.** UV−vis spectra were recorded on a Shimadzu UV-2401 PC spectrophotometer in CHCl$_3$/CH$_3$CN (9:1 v/v). Polymer films were prepared by compression molding in a Carver CE Press at 90 °C, 3 tons of pressure, 5 min in the case of UPy-PEB-UPy and 120 °C, 3 tons of pressure, 20 min in the case of [Zn(Mebip-PEB-Mebip)]-(NTf$_2$)$_2$ and [Fe(Mebip-PEB-Mebip)](ClO$_4$)$_2$ unless specified otherwise. Dynamic mechanical thermal analyses (DMTA) were conducted under N$_2$ on a TA Instruments DMA Q800 with a heating rate of 3 °C/min, a frequency of 1 Hz, and an amplitude of 15 μm in the range of −70 to 250 °C, unless indicated otherwise. Reported mechanical data are averages of 3−10 independent experiments, and all errors are standard deviations. The small-angle X-ray scattering (SAXS) spectra were collected on a S-MAX3000 instrument with a pinhole camera (Rigaku Innovative Technologies, Auburn Hills, MI). The samples were kept under vacuum at room temperature during the measurements. Raw data were processed according to standard procedures, and the scattering spectra are presented as a function of the momentum transfer $q = 4\pi\lambda^{-1} \sin(\theta/2)$, where θ is the scattering angle and λ = 0.1524 nm is the photon wavelength. Scanning transmission electron microscopy (STEM) was performed using a JEOL JEM-2100F microscope operated at 200 kV on unstained sections cut with a Leica UCT cryo-ultramicrotome. High-angle annular dark field (HAADF) STEM images were collected using a Gatan Model 806 HAADF-STEM detector with a 40 μm condenser aperture.

UV−Vis Titrations of UPy-PEB-UPy and Mebip-PEB-Mebip. A solution of UPy-PEB-UPy (0.14 mg, 20 μM) in a CHCl$_3$/CH$_3$CN mixture (9:1 v/v, 2 mL) was titrated with 25 μL aliquots of Zn(NTf$_2$)$_2$ (416 μM) in CHCl$_3$/CH$_3$CN (9:1 v/v). The addition was done incrementally, and after each aliquot addition of the metal solution the sample was characterized by UV−vis spectroscopy. The absorption at 354 nm was plotted against the concentration of Zn^{2+}. The experiment was repeated with UPy-PEB-UPy (0.13 mg, 18.6 μM) and Fe(ClO$_4$)$_2$ (454 μM) in the same solvent mixture. UV−vis titrations of Mebip-PEB-Mebip with solutions of Zn(NTf$_2$)$_2$ or Fe(ClO$_4$)$_2$ were performed using the previously reported procedures.[18]

UV−Vis Titration of a Mixture of Mebip-PEB-Mebip and UPy-PEB-UPy. A solution of Mebip-PEB-Mebip (0.16 mg, 18.1 μM) and UPy-PEB-UPy (0.13 mg, 18.6 μM) in a CHCl$_3$/CH$_3$CN mixture (9:1 v/v, 2 mL) was titrated with 25 μL aliquots of Zn(NTf$_2$)$_2$ (416 μM) in CHCl$_3$/CH$_3$CN (9:1 v/v, 10 mL). The addition was done incrementally, and after each aliquot addition of the metal solution the sample was characterized by UV−vis spectroscopy. The absorption at 354 nm was plotted against the concentration of Zn^{2+}. The experiment was repeated with a solution of Mebip-PEB-Mebip (0.17 mg, 19.3 μM) and UPy-PEB-UPy (0.13 mg, 18.6 μM) and a solution of Fe(ClO$_4$)$_2$ (416 μM), and the absorption at 354 nm was plotted against the concentration of Fe^{2+}.

UV−Vis Titration of Metallosupramolecular Polymers with UPy-PEB-UPy. A solution of [Zn(Mebip-PEB-Mebip)](NTf$_2$)$_2$ (0.62 mg, 70.5 μM) in a CHCl$_3$/CH$_3$CN mixture (9:1 v/v, 2 mL) was titrated with 100 μL (0.1 equiv) aliquots of UPy-PEB-UPy (4.93 mg, 141 μM) in CHCl$_3$/CH$_3$CN (9:1 v/v). The addition was done incrementally, and after each aliquot addition the sample was characterized by UV−vis spectroscopy. The absorption at 354 nm was plotted against the concentration of UPy-PEB-UPy. The experiment was repeated with solutions of [Fe(Mebip-PEB-Mebip)]-(ClO$_4$)$_2$ (0.63 mg, 71.6 μM) and UPy-PEB-UPy (4.93 mg, 141 μM).

Preparation of {[Zn(Mebip-PEB-Mebip)](NTf$_2$)$_2$}$_{1.0}$(UPy-PEB-UPy)$_x$ and {[Fe(Mebip-PEB-Mebip)](ClO$_4$)$_2$}$_{1.0}$(UPy-PEB-UPy)$_x$ Blends and Processing of Thin Films. A representative procedure for the blend {[Zn(Mebip-PEB-Mebip)](NTf$_2$)$_2$}$_{1.0}$(UPy-PEB-UPy)$_{1.0}$ is provided, which serves as an example for the preparation of all the other compositions of this blend system. To a stirred solution of Mebip-PEB-Mebip (251 mg, 0.06 mmol) in CHCl$_3$ (3 mL), a solution of Zn(NTf$_2$)$_2$ (3.18 mL, 0.06 mmol) in anhydrous CH$_3$CN was added. The mixture was stirred for 20 min, and a solution of UPy-PEB-UPy (199 mg, 0.06 mmol) in CHCl$_3$ (3 mL) corresponding to 1 equiv of Mebip-PEB-Mebip was added and stirred for an additional 30 min. Thin films of a thickness of 150−250 μm were prepared by casting the
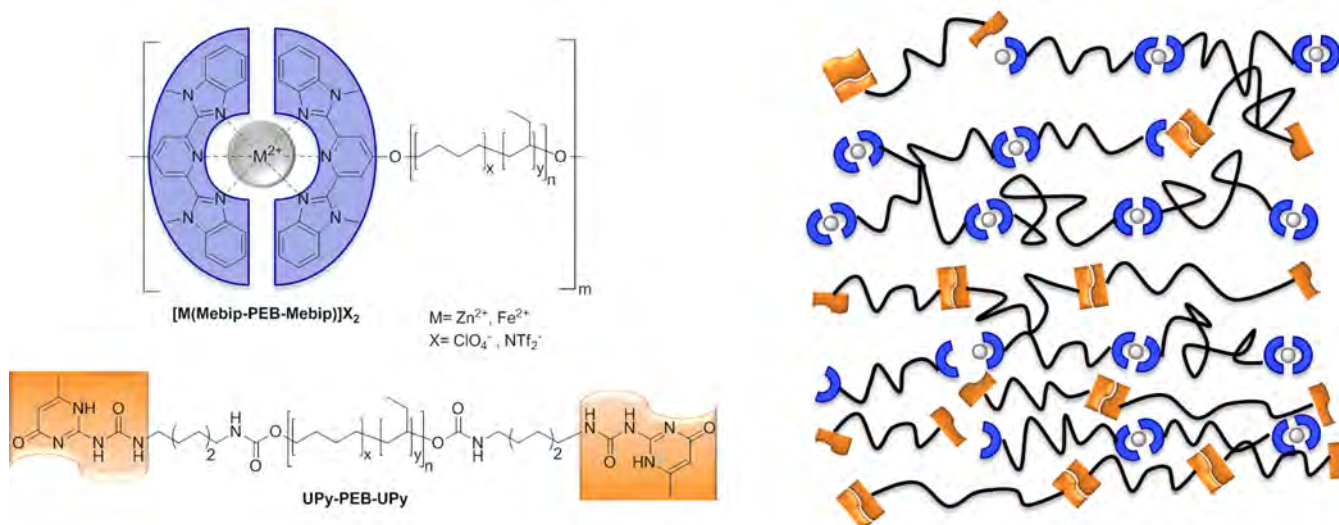
Figure 1. Schematic representation of the metallopolymers [Zn(Mebip-PEB-Mebip)](NTf$_2$)$_2$ and [Fe(Mebip-PEB-Mebip)](ClO$_4$)$_2$, the hydrogen-bonded polymer UPy-PEB-UPy, and the resulting blends {[Zn(Mebip-PEB-Mebip)](NTf$_2$)$_2$}$_{1.0}$(NTf$_2$)$_2$(UPy-PEB-UPy)$_x$ and {[FeMebip-PEB-Mebip](ClO$_4$)$_2$}$_{1.0}$(UPy-PEB-UPy)$_x$.

solution into a Teflon Petri dish of 100 mm, drying the sample at 40 °C in vacuum oven for 1 day, and subsequent compression molding the resulting film at 80 °C for 20−30 min. Films based on the blend {[Fe(Mebip-PEB-Mebip)](ClO$_4$)$_2$}$_{1.0}$(UPy-PEB-UPy)$_{0.7}$ were made by the same process, using a solution of Mebip-PEB-Mebip (298 mg, 0.07 mmol) and a solution of Fe(ClO$_4$)$_2$ (463 μL, 0.07 mmol) in anhydrous CH$_3$CN. Other compositions of this blend system were made in an analogous manner.

Swelling Behavior of Polymer Films. A representative procedure is provided. The swelling behavior of a {[Fe(Mebip-PEB-Mebip)](ClO$_4$)$_2$}$_{1.0}$(UPy-PEB-UPy)$_{0.7}$ blend film was measured in CH$_3$CN. Samples of thin films (20 mg, 20 mm × 5 mm × 150 μm) were immersed in the solvent at room temperature for 1 day, and the degree of swelling was determined by measuring the weight of the samples pre- and postswelling:

$$\text{degree of swelling (\%)} = \frac{\text{mass of swollen} - \text{mass of dry sample}}{\text{mass of dry sample}} \times 100$$

To minimize the error in measuring the degree of swelling, samples were placed on filter paper to wick excess CH$_3$CN from the surface before they were weighed. Reported results represent averages of three independent measurements.

RESULTS AND DISCUSSION

Preparation of Macromonomers and Supramolecular Polymers. Supramolecular macromonomers based on a telechelic poly(ethylene-co-butylene) (PEB) end-functionalized with either metal-coordinating 2,6-bis(1′-methylbenz-imidazolyl)pyridine (Mebip) ligands (Mebip-PEB-Mebip) or with a hydrogen-bonding ureidopyrimidinone, UPy, motif (UPy-PEB-UPy) were synthesized as previously described (Figures S12−S14).[6,18] MSPs of the sum formula [Zn-(Mebip-PEB-Mebip)](NTf$_2$)$_2$ and [Fe(Mebip-PEB-Mebip)]-(ClO$_4$)$_2$ were prepared by coordination of the Mebip-PEB-Mebip macromonomer to 1 equiv of an appropriate metal salt, i.e., zinc(II) bistriflimide or iron(II) perchlorate (Figure 1).

Determination of the Orthogonality of the Supramolecular Interactions by UV−Vis Titration. To explore the degree of orthogonality of the metal-coordination and hydrogen-bonding supramolecular motifs used here, a series of titrations were performed in which possible interactions between the MSPs [M(Mebip-PEB-Mebip)](X)$_2$ and the

UPy-PEB-UPy polymer were probed by UV−vis spectroscopy. Thus, UPy-PEB-UPy and Mebip-PEB-Mebip were individually as well as in equimolar combination titrated with aliquots of Zn(NTf$_2$)$_2$ and Fe(ClO$_4$)$_2$. Titrations of the preformed MSPs with UPy-PEB-UPy were also performed.

As previously reported,[17,18] Mebip-PEB-Mebip features an absorbance band of the ligand with a maximum (λ_{max}) at 313 nm (Figures S1). Upon coordination with Zn(NTf$_2$)$_2$, the absorbance signature of the newly formed ligand-to-metal charge transfer (LMCT) transition displays a λ_{max} around 354 nm (Figure S1). The intensity of the two bands decreases (313 nm) or increases (354 nm) as the monomer is titrated with the metal salt, and a plot of the absorbance at 354 nm (and likewise 313 nm) as a function of the Zn^{2+}:macromonomer ratio (Figure 2b) shows that the optical changes discontinue once the stoichiometry is equimolar, i.e., at the point when the MSP is fully formed. Using a similar procedure, UPy-PEB-UPy was titrated with aliquots of Zn(NTf$_2$)$_2$ to explore if (in this case undesired) interactions between Zn^{2+} and the UPy motifs can occur. UPy-PEB-UPy exhibits an absorbance spectrum that is characteristic of the UPy unit with λ_{max} at 265 nm (Figure S2). Upon addition of Zn(NTf$_2$)$_2$ an absorbance band with λ_{max} at 354 nm develops, which we interpret as the result of the coordination of Zn^{2+} to the UPy groups (Figure S2). Using these titrations as a reference point, aliquots of Zn(NTf$_2$)$_2$ were added to an equimolar mixture of Mebip-PEB-Mebip and UPy-PEB-UPy in CH$_3$CN:CHCl$_3$ (9:1 v/v), and spectroscopic changes were monitored by UV−vis spectroscopy (Figure 2a). In the absence of Zn^{2+}, the absorption spectrum (Figure 2a) shows a superposition of the spectra of the two individual components. Upon addition of Zn(NTf$_2$)$_2$, a bathochromic shift and the characteristic signature of the Mebip-Zn^{2+} LMCT can be observed (Figure 2a). The absorption spectrum exhibits two isosbestic points at 265 and 325 nm, reflecting a well-defined equilibrium between the free ligands (UPy and Mebip) and their coordination complexes with Zn^{2+}. A plot of the absorbance at 354 nm (signature of the LMCT) as a function of the Zn^{2+}:macromonomer ratio (Figure 2b) shows a behavior that is in between those of the individual components. While the absorbance continually increases, the increase is less in
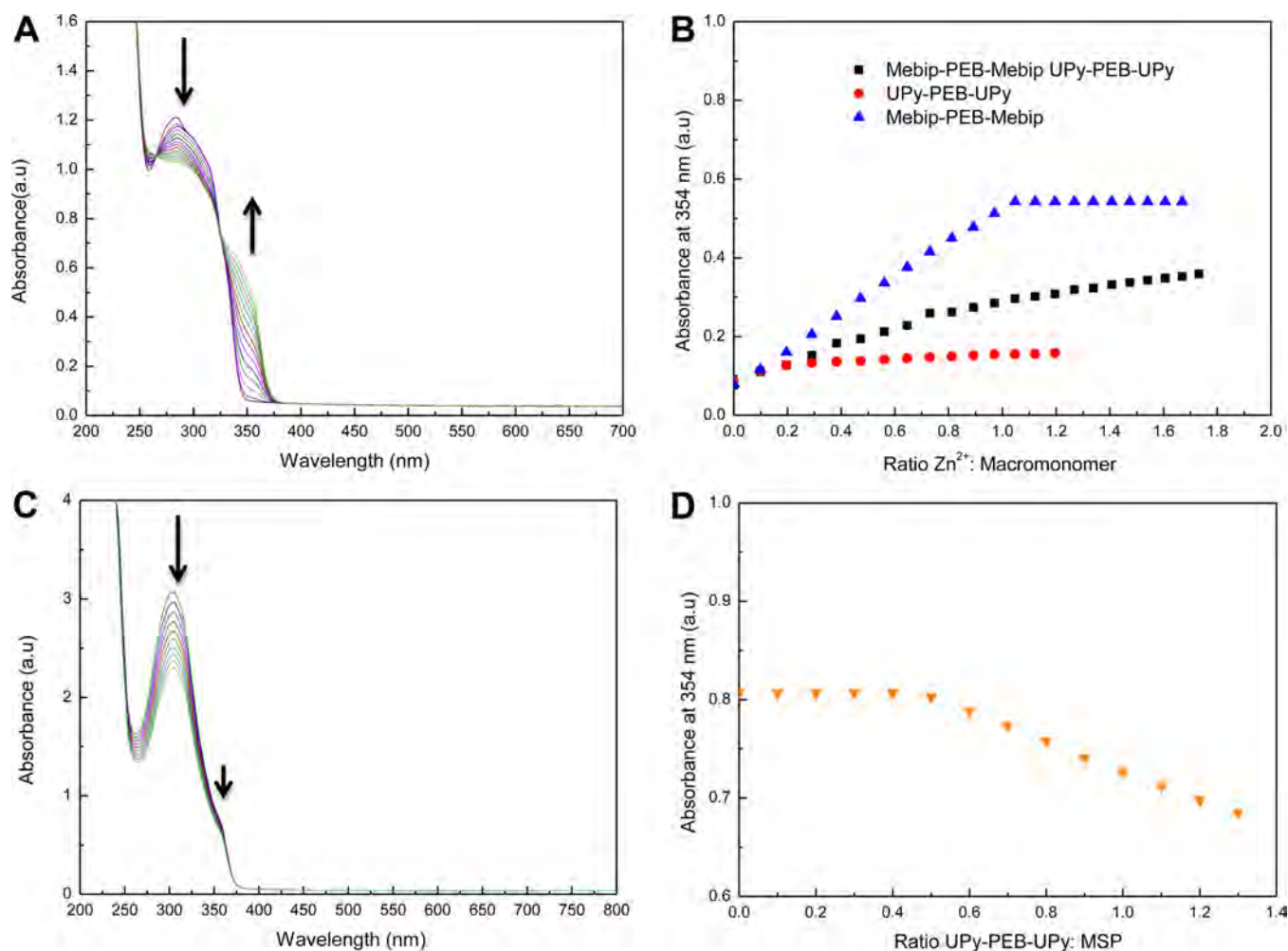
Figure 2. (A) UV−vis absorption spectra acquired upon titration of a solution containing a mixture of Mebip-PEB-Mebip and UPy-PEB-UPy (18 μM each) with $Zn(NTf_2)_2$ (416 μM). (B) Absorption at 354 nm of the spectra shown in (A) as a function of the $Zn(NTf_2)_2$:macromonomer ratio (■); also shown are the corresponding data for the titrations of solutions containing only Mebip-PEB-Mebip (18 μM, ▲) or UPy-PEB-UPy (18 μM, ●). (C) UV−vis absorption spectra acquired upon titration of a solution of the preformed metallosupramolecular polymer [Zn(Mebip-PEB-Mebip)]$(NTf_2)_2$ (70 μM) with UPy-PEB-UPy (141 μM). (D) Absorption at 354 nm of the spectra shown in (C) as a function of the UPy-PEB-UPy:MSP ratio (▼). All solutions were made in a 9:1 v/v $CHCl_3$/CH_3CN mixture.

comparison to the titration of the neat Mebip-PEB-Mebip, and no end point at the Zn^{2+}:macromonomer ratio of 1:1 is observed (Figure 2b, Figures S1 and S2). A titration of the preformed [Zn(Mebip-PEB-Mebip)]$(NTf_2)_2$ with aliquots of UPy-PEB-UPy in $CHCl_3$:CH_3CN (9:1 v/v) was also performed. As can be seen from the data shown in Figure 2c, the absorbance of the Mebip-Zn^{2+} LMCT (λ_{max} = 354 nm) did not vary upon addition of 0.5 equiv of UPy-PEB-UPy, suggesting a preference for the dimerization of the UPy motifs (association constant K_a = 6 × 10^7 M^{-1} in $CHCl_3$[25,26]) over the disruption of the coordination of Zn^{2+} to Mebip-PEB-Mebip (K_a = 10^5 M^{-1} in $CHCl_3$[27−29]). However, upon further increase of the UPy-PEB-UPy concentration, the absorbance at 354 nm decreased, likely due to reshuffling of UPy and Mebip moieties with Zn^{2+} (Figure 2c,d). Thus, these results suggest that Zn^{2+} shows no clear preference in coordination with the Mebip or UPy motifs, and due to the dynamic nature of both Zn-Mebip and UPy-UPy interactions, a statistical mixture of Zn-Mebip, UPy-UPy, and Zn-UPy is also formed if preformed materials are combined. In other words the Zn^{2+}-based supramolecular polymer and the hydrogen-bonded UPy-PEB-UPy do not show the targeted orthogonal binding.

In an attempt to increase the orthogonality of the present materials, Zn^{2+} was substituted with a Fe^{2+} salt because Zn^{2+} tridentate amine complexes are generally more labile than the corresponding Fe^{2+} complexes.[29] Again, a series of UV−vis titrations were performed to monitor the interactions between Mebip-PEB-Mebip, UPy-PEB-UPy, and $Fe(ClO_4)_2$. As a control, aliquots of $Fe(ClO_4)_2$ were added to the macro-monomer Mebip-PEB-Mebip, and the change of absorbance was monitored. Upon coordination of Mebip with $Fe(ClO_4)_2$, the intensity of the Mebip absorption band around 313 nm decreases, and the Fe^{2+}-Mebip complex thus formed causes new absorption bands with λ_{max} at 341 and 354 nm and a diagnostic metal-to-ligand charge transfer (MLCT) transition with λ_{max} = 565 nm (Figure S3). We also titrated UPy-PEB-UPy with aliquots of $Fe(ClO_4)_2$, and upon addition of $Fe(ClO_4)_2$ the intensity of the absorption bands centered at 265 and 354 nm increased with increasing iron content (Figure S4). Using these titrations as reference points, aliquots of $Fe(ClO_4)_2$ were added to an equimolar mixture of Mebip-PEB-Mebip and UPy-PEB-UPy, and the change in absorbance was monitored by UV−vis spectroscopy (Figure 3a). As can be seen from the data presented in Figure 3, upon coordination with $Fe(ClO_4)_2$ the
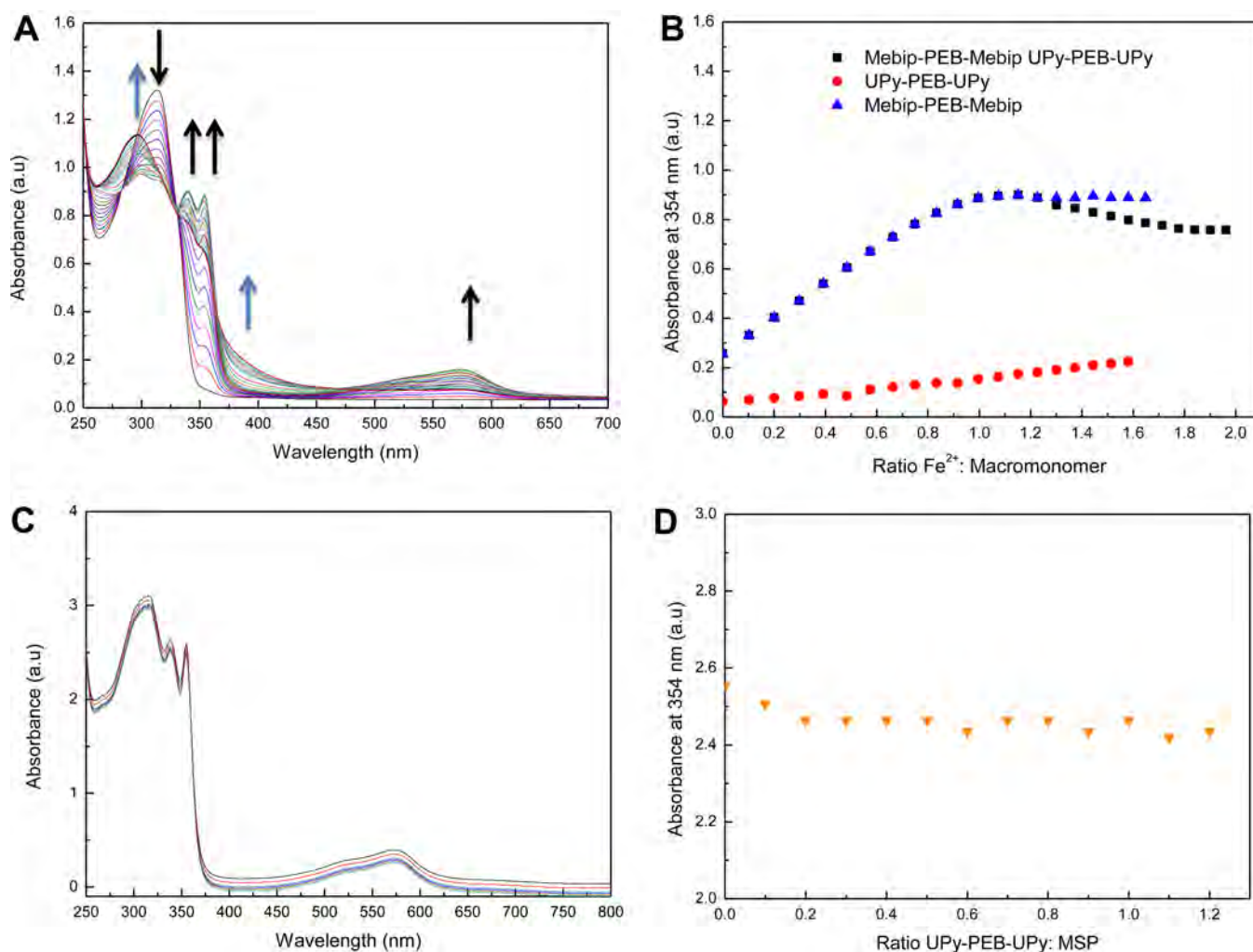
Figure 3. (A) UV−vis absorption spectra acquired upon titration of a solution containing a mixture of Mebip-PEB-Mebip and UPy-PEB-UPy (19 μM each) with $Fe(ClO_4)_2$ (416 μM). The black arrow and blue arrow indicate increases of bands associated with Mebip-Fe and UPy-Fe complexes, respectively. (B) Absorption at 354 nm of the spectra shown in (A) as a function of the $Fe(ClO_4)_2$:macromonomer ratio (■); also shown are the corresponding data for the titrations of solutions containing only Mebip-PEB-Mebip (19 μM, ▲) or UPy-PEB-UPy (19 μM, ●). (C) UV−vis absorption spectra acquired upon titration of a solution of the preformed metallosupramolecular polymer [Fe(Mebip-PEB-Mebip)]$(ClO_4)_2$ (72 μM) with UPy-PEB-UPy (141 μM). (D) Absorption at 354 nm of the spectra shown in (C) as a function of the UPy-PEB-UPy:MSP ratio (▼). All solutions were prepared in a 9:1 v/v $CHCl_3/CH_3CN$ mixture.

absorbance spectrum in the presence of both supramolecular moieties exhibits a slight bathochromic shift for the diagnostic transitions of the Fe^{2+}-Mebip complex, and a decrease of the Mebip absorbance is also observed. In addition, an absorbance maximum at 275 nm corresponding to Fe^{2+}-UPy interactions and a λ_{max} at 395 nm corresponding to unstacked UPy units are also observed in the titration (Figure 3a,b and Figure S4).[30,31] A plot of the absorbance at 354 nm as a function of Fe^{2+}:macromonomer ratio shows a strong tendency for the formation of the metallosupramolecular polymer [Fe(Mebip-PEB-Mebip)]$(ClO_4)_2$, as is observed in the titration of neat Mebip-PEB-Mebip (i.e., in the absence of UPy-PEB-UPy) with Fe^{2+} salts (Figure 3b and Figure S3).[18] The data show a discontinuity of the absorbance change at a Fe^{2+}:Mebip-PEB-Mebip ratio of 1:1, corresponding to a Fe^{2+}:Mebip ratio of 1:2 (Figure 3b). Further addition of $Fe(ClO_4)_2$ leads to the appearance of a new absorption bands with maxima λ_{max} at 275 and 395 nm, which are characteristic of the coordination of Fe^{2+} to UPy motifs. These findings suggest that the presence of UPy-PEB-UPy does not disrupt the formation of [Fe(Mebip-

PEB-Mebip)]$(ClO_4)_2$; only after all of the Mebip ligands have been coordinated with iron(II) ions does the coordination of Fe^{2+}-UPy commence. This is likely due to the strong coordination of Fe^{2+} to the Mebip ligand ($K_a = 10^{13}$ M^{-1}),[28] which is much more pronounced than the UPy dimerization in $CHCl_3$ ($K_a = 6 \times 10^7$ M^{-1}). Moreover the addition of UPy-PEB-UPy aliquots to a preformed [Fe(Mebip-PEB-Mebip)]-$(ClO_4)_2$ polymer does not cause a significant change in the absorption spectra (Figure 3c,d). Collectively, these data suggest that metal−ligand coordination (Fe^{2+}-Mebip) and hydrogen-bonding (UPy-UPy dimers) interactions are indeed orthogonal.

Preparation of Blend Films and Morphological Characterization. Thin films of [Zn(Mebip-PEB-Mebip)]-$(NTf_2)_2$, [Fe(Mebip-PEB-Mebip)]$(ClO_4)_2$, and UPy-PEB-UPy as controls and blends of [Zn(Mebip-PEB-Mebip)]$(NTf_2)_2$/(UPy-PEB-UPy) and [Fe(Mebip-PEB-Mebip)]$(ClO_4)_2$/(UPy-PEB-UPy) (referred to as {[M(Mebip-PEB-Mebip)]-$(X)_2\}_{1.0}$(UPy-PEB-UPy)$_x$ (x = 1−0.2 equiv; M = Zn, Fe; X = NTf_2^-, ClO_4^-)) were prepared to explore the structure−

property relationship of these materials, in particular the influence of the orthogonal supramolecular motifs and the composition on the morphology, mechanical properties, and stimuli-responsive behavior. For all compositions, thin films with a thickness of 150−250 μm were produced by combining all building blocks in a mixture of $CHCl_3$ and CH_3CN, solution casting and evaporation of the solvent, and subsequent compression molding at elevated temperature (see Experimental Section for details). Their morphology was analyzed by small-angle X-ray scattering (SAXS). Previous work on [Zn(Mebip-PEB-Mebip)](NTf$_2$)$_2$ revealed microphase-segregated lamellar morphologies in which the metal−ligand complexes form a hard phase that physically cross-links the soft domains formed by the poly(ethylene-*co*-butylene) core.[17,18,32] The SAXS pattern of UPy-PEB-UPy homopolymer films also reveals a short-range order that points to a morphology of densely packed nanofibers, as reported by Meijer et al. (Figure 4).[15,30]
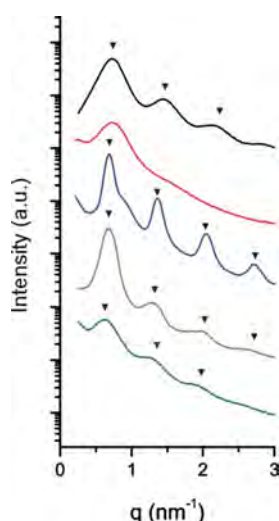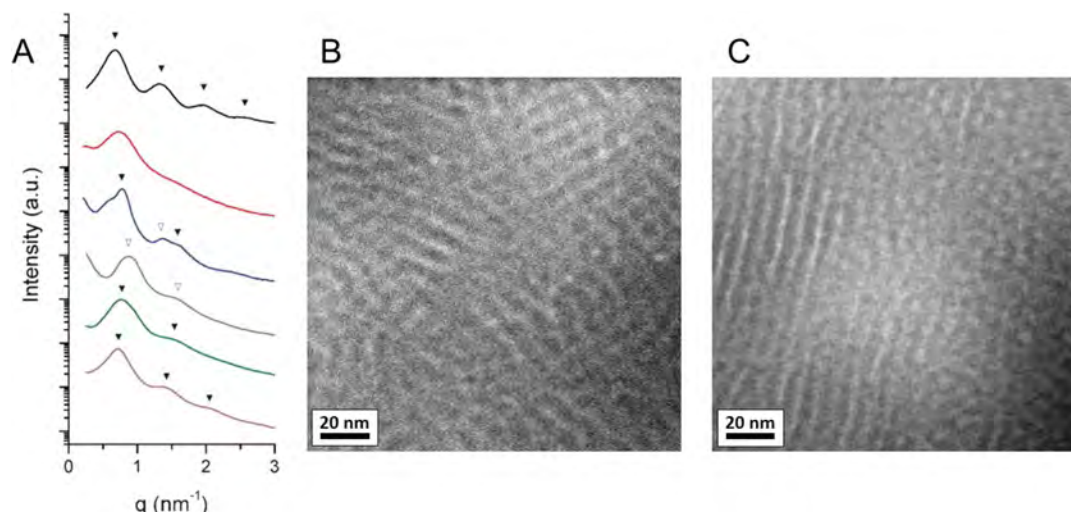

Figure 4. SAXS spectra of the neat metallosupramolecular polymer [Zn(Mebip-PEB-Mebip)](NTf$_2$)$_2$ (black), the neat UPy-PEB-UPy (red), blends {[Zn(Mebip-PEB-Mebip)](NTf$_2$)$_2$}$_{1.0}$(NTf$_2$)$_2$(UPy-PEB-UPy)$_{1.0}$ (blue), {[Zn(Mebip-PEB-Mebip)](NTf$_2$)$_2$}$_{1.0}$-(NTf$_2$)$_2$(UPy-PEB-UPy)$_{0.5}$ (gray), and {[Zn(Mebip-PEB-Mebip)]-(NTf$_2$)$_2$}$_{1.0}$(UPy-PEB-UPy)$_{0.2}$ (green). The triangles show the scattering maxima corresponding to lamellar morphology. The scattering spectra of the supramolecular polymers blends have been vertically shifted for visualization and clarity.

The SAXS spectra of {[Zn(Mebip-PEB-Mebip)](NTf$_2$)$_2$}$_{1.0}$-(UPy-PEB-UPy)$_x$ (x = 1, 0.5, 0.2 equiv) blends with varying UPy-PEB-UPy content show equidistant Bragg diffraction peaks that are clearly discernible up to the third order (Figure 4). These features mirror those of the neat metallosupramolecular polymer [Zn(Mebip-PEB-Mebip)](NTf$_2$)$_2$ and confirm that the blends adopt a lamellar morphology with considerable long-range order.[17,18] The equimolar blend {[Zn(Mebip-PEB-Mebip)](NTf$_2$)$_2$}$_{1.0}$(UPy-PEB-UPy)$_{1.0}$ also displays scattering features corresponding to the neat UPy-PEB-UPy (densely packed fibers), suggesting that at high UPy-PEB-UPy concentration phase-segregation effects may be at play.

The SAXS spectra of {[Fe(Mebip-PEB-Mebip)]-(ClO$_4$)$_2$}$_{1.0}$(UPy-PEB-UPy)$_x$ (x = 1, 0.7, 0.5, and 0.3 equiv) blends with varying UPy-PEB-UPy content also show distinct Bragg diffraction peaks up to the second order, which mirror

those of the neat [Fe(Mebip-PEB-Mebip)](ClO$_4$)$_2$ and suggest that most of these materials also adopt lamellar morphologies with significant long-range order (Figure 5). However, the blend of equimolar {[Fe(Mebip-PEB-Mebip)]-(ClO$_4$)$_2$}$_{1.0}$(UPy-PEB-UPy)$_{1.0}$ shows a complex scattering pattern. Fitting of the data suggests that this is likely due to the presence of both lamellar and cylinder morphologies, whereas the {[Fe(Mebip-PEB-Mebip)](ClO$_4$)$_2$}$_{1.0}$(UPy-PEB-UPy)$_{0.7}$ blend adopts a cylindrical morphology (Figure 5a). TEM images of the [Fe(Mebip-PEB-Mebip)](ClO$_4$)$_2$ homopolymer control and {[Fe(Mebip-PEB-Mebip)]-(ClO$_4$)$_2$}$_{1.0}$(UPy-PEB-UPy)$_{0.7}$ confirm the presence of lamellar and hexagonally packed cylinders morphologies, respectively (Figure 5b,c). Similar to the Zn-based blends, the equimolar {[Fe(Mebip-PEB-Mebip)](ClO$_4$)$_2$}$_{1.0}$(UPy-PEB-UPy)$_{1.0}$ blend, which also presents scattering features corresponding to the neat UPy-PEB-UPy (densely packed fibers), suggesting that both a long-range lamellar morphology and short-range packed fibers are present in this composition (Figure S5). Interestingly, when the blends of {[Fe(Mebip-PEB-Mebip)]-(ClO$_4$)$_2$}$_{1.0}$(UPy-PEB-UPy)$_{1.0}$ and {[Fe(Mebip-PEB-Mebip)]-(ClO$_4$)$_2$}$_{1.0}$(UPy-PEB-UPy)$_{0.7}$ were analyzed by SAXS after 2 months, different morphologies were observed, suggesting that the samples slowly change over prolonged periods of time (Figure S5). The mechanism and kinetics of this spontaneous morphological shift are unclear at this point and will be the focus of future studies. All scattering patterns were isotropic, indicating that the domains are not oriented.

Mechanical Properties and Thermoresponsive Behavior. The mechanical properties of the supramolecular polymer blends were explored using dynamic mechanical thermal analysis (DMTA) (Figure 6, Table 1) and at room temperature by means of tensile testing (Table S1 and Figure S10). Similar results to previously reported data were obtained for neat [Zn(Mebip-PEB-Mebip)](NTf$_2$)$_2$ and UPy-PEB-UPy homopolymer films, where a glassy behavior is observed below −23 °C, and the materials display a tensile storage modulus (E') of ∼2 and ∼1.5 GPa, respectively (Figure 6).[6,17,18] Above the glass transition a broad rubbery plateau is observed, and at 25 °C [Zn(Mebip-PEB-Mebip)](NTf$_2$)$_2$ displays a storage modulus of ∼100 MPa, whereas UPy-PEB-UPy has a storage modulus of ∼9 MPa. This behavior is consistent with supramolecular thermoplastic elastomers with microphase-segregated morphologies (Figure 4) in which the UPy stacking and metal−ligand motifs phase separate from the amorphous PEB soft phase to form hard phases that serve as physical cross-links. The [Zn(Mebip-PEB-Mebip)](NTf$_2$)$_2$ and UPy-PEB-UPy homopolymers display a temperature of failure, where the hard phases of the material melt resulting in catastrophic failure, at 250 and 70 °C, respectively. The DMTA traces of {[Zn(Mebip-PEB-Mebip)](NTf$_2$)$_2$}$_{1.0}$(UPy-PEB-UPy)$_x$ blends display an intermediate behavior. The storage modulus (10−21 MPa at 25 °C) in the rubbery regime appears to increase with the [Zn(Mebip-PEB-Mebip)](NTf$_2$)$_2$ content (Figure 6 and Table 1), but even at a 1:1 mixture of the metallopolymer and the hydrogen-bonded material, the stiffness is only a fraction of that of the neat [Zn(Mebip-PEB-Mebip)](NTf$_2$)$_2$ polymer. The relatively low E' of the supramolecular blends can be attributed to a decrease of the Zn^{2+}-Mebip complex concentration due to the formation of a statistical mixture of supramolecular interactions between Zn^{2+}-Mebip, Zn^{2+}-UPy, and UPy-UPy (*vide supra*). Additionally, the failure temperature (T_{fail}) of the supramolecular blends decreases in comparison to the neat

Figure 5. (A) SAXS spectra of the metallosupramolecular polymer $[Fe(Mebip-PEB-Mebip)](ClO_4)_2$ (black), the neat UPy-PEB-UPy (red), blends $\{[Fe(Mebip-PEB-Mebip)](ClO_4)_2\}_{1.0}(UPy-PEB-UPy)_{1.0}$ (blue), $\{[Fe(Mebip-PEB-Mebip)](ClO_4)_2\}_{1.0}(UPy-PEB-UPy)_{0.7}$ (gray), $\{[Fe(Mebip-PEB-Mebip)](ClO_4)_2\}_{1.0}(UPy-PEB-UPy)_{0.5}$ (green), and $\{[Fe(Mebip-PEB-Mebip)](ClO_4)_2\}_{1.0}(UPy-PEB-UPy)_{0.3}$ (purple). The closed and open triangles show the scattering maxima corresponding to lamellar and cylindrical morphologies, respectively. The scattering spectra of the supramolecular polymers blends have been vertically shifted for visualization and clarity. (B) HAADF-STEM image of $[Fe(Mebip-PEB-Mebip)](ClO_4)_2$, showing overlapping lamellar regions. (C) HAADF-STEM image of $\{[Fe(Mebip-PEB-Mebip)](ClO_4)_2\}_{1.0}(UPy-PEB-UPy)_{0.7}$, showing hexagonally packed cylinder structures.
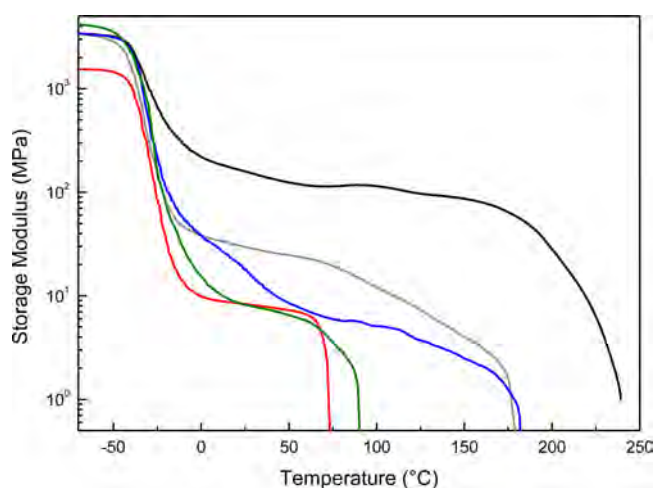
Figure 6. Representative dynamic mechanical thermal analysis (DMTA) traces of the neat metallosupramolecular polymer $[Zn(Mebip-PEB-Mebip)](NTf_2)_2$ (black), the neat UPy-PEB-UPy (red), and the blends $\{[Zn(Mebip-PEB-Mebip)](NTf_2)_2\}_{1.0}(UPy-PEB-UPy)_{1.0}$ (blue), $\{[Zn(Mebip-PEB-Mebip)](NTf_2)_2\}_{1.0}(UPy-PEB-UPy)_{0.5}$ (gray), and $\{[Zn(Mebip-PEB-Mebip)](NTf_2)_2\}_{1.0}(UPy-PEB-UPy)_{0.2}$ (green). The experiments were conducted at a heating rate of 3 °C/min and a frequency of 1 Hz under N_2.
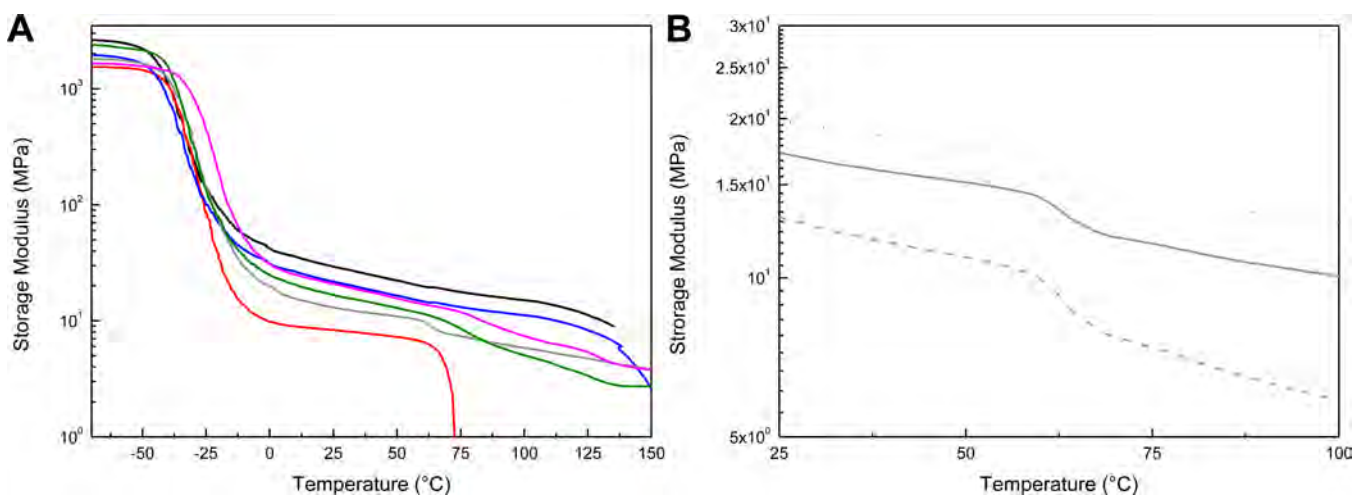
metallosupramolecular polymer $[Zn(Mebip-PEB-Mebip)](NTf_2)_2$ from around 200 to 175 °C for both the $\{[Zn(Mebip-PEB-Mebip)](NTf_2)_2\}_{1.0}(UPy-PEB-UPy)_{1.0}$ blend and $\{[Zn(Mebip-PEB-Mebip)](NTf_2)_2\}_{1.0}(UPy-PEB-UPy)_{0.5}$ (Figure 6). Surprisingly, the blend with the lowest UPy-PEB-UPy content, $\{[Zn(Mebip-PEB-Mebip)](NTf_2)_2\}_{1.0}(UPy-PEB-UPy)_{0.2}$, displays a T_{fail} of 80 °C, which is only slightly higher than that of UPy-PEB-UPy (70 °C). Stress−strain experiments conducted at 25 °C reveal Young's moduli that mirror this trend and result in a maximum stress at break of 1.6 MPa for UPy-PEB-UPy, 4.6 MPa for $[Zn(Mebip-PEB-Mebip)](NTf_2)_2$, and decreasing values for the $\{[Zn(Mebip-PEB-Mebip)]-$

$(NTf_2)_2\}_{1.0}(UPy-PEB-UPy)_x$ blends as the UPy-PEB-UPy content is decreased (2.3 MPa = 1.0 equiv; 0.8 MPa = 0.7 equiv; 0.3 MPa = 0.2 equiv) (Figure S10 and Table S1). Taking into consideration the results from SAXS and DMTA studies, we conclude that the mechanical properties of the Zn-based supramolecular polymer blends are largely driven by the extent of phase segregation. For instance, samples with well-defined lamellar morphologies, $\{[Zn(Mebip-PEB-Mebip)]-$$(NTf_2)_2\}_{1.0}(UPy-PEB-UPy)_{1.0}$ and $\{[Zn(Mebip-PEB-Mebip)]-$$(NTf_2)_2\}_{1.0}(UPy-PEB-UPy)_{0.5}$, exhibit a rather high T_{fail} of ca. 175 °C and display the highest E' in the rubbery state, even though the UPy-PEB-UPy content is relatively high. Conversely, $\{[Zn(Mebip-PEB-Mebip)](NTf_2)_2\}_{1.0}(UPy-PEB-$$UPy)_{0.2}$, which contains only 1 mol equiv of the hydrogen-bonded polymer, exhibits a comparably low degree of long-range order according to the SAXS data, and the mechanical properties are similar to those of the neat UPy-PEB-UPy (Figures 4 and 6, Table 1).

The mechanical characteristics of $\{[Fe(Mebip-PEB-Mebip)]-$$(ClO_4)_2\}_{1.0}(UPy-PEB-UPy)_x$ (x = 0.3, 0.5, 0.7, and 1.0 equiv) thin films were also explored using DMTA (Figure 7 and Table 1) and tensile testing at room temperature (Table S1 and Figure S11). The properties of the neat $[Fe(Mebip-PEB-Mebip)](ClO_4)_2$ match previously reported data well, where a glassy behavior is observed below −23 °C with an E' of ~2 GPa, and the material displays an E' of ~28 MPa at 25 °C (Figure 7). The failure temperature of $[Fe(Mebip-PEB-Mebip)](ClO_4)_2$ is ca. 180 °C.[16] The $\{[Fe(Mebip-PEB-Mebip)](ClO_4)_2\}_x$ blends display a small increase of E' in comparison to UPy-PEB-UPy homopolymer in the rubbery regime (Figure 7 and Table 1). Upon closer examination of the DMTA traces, $\{[Fe(Mebip-PEB-Mebip)]-$$(ClO_4)_2\}_{1.0}(UPy-PEB-UPy)_x$ blends with a UPy content of x = 0.3, 0.5, and 0.7 equiv display a steplike transition in the range 60−80 °C (Figure 7). This drop of the storage modulus is characteristic to the melting of the hydrogen-bonded UPy dimers.[33] The mechanical properties can be related to the

Table 1. Mechanical Properties of Supramolecular Polymer Blends of UPy-PEB-UPy, [Zn(Mebip-PEB-Mebip)](NTf$_2$)$_2$, and [Fe(Mebip-PEB-Mebip)](ClO$_4$)$_2$[a]

| supramolecular polymer	storage modulus (MPa) at −70 °C	storage modulus (MPa) at 25 °C	failure temp (°C)
UPy-PEB-UPy	1744 ± 160	7 ± 2	60−80
[Zn(Mebip-PEB-Mebip)](NTf$_2$)$_2$	2210 ± 113	100 ± 8	230−250
{[Zn(Mebip-PEB-Mebip)](NTf$_2$)$_2$}$_{1.0}$(UPy-PEB-UPy)$_{1.0}$	2532 ± 365	21 ± 6	160−180
{[Zn(Mebip-PEB-Mebip)](NTf$_2$)$_2$}$_{1.0}$(UPy-PEB-UPy)$_{0.5}$	2870 ± 372	18 ± 5	160−180
{[Zn(Mebip-PEB-Mebip)](NTf$_2$)$_2$}$_{1.0}$(UPy-PEB-UPy)$_{0.2}$	3142 ± 785	9 ± 3	80−100
[Fe(Mebip-PEB-Mebip)](ClO$_4$)$_2$	1437 ± 103	28 ± 3	160−190
{[Fe(Mebip-PEB-Mebip)](ClO$_4$)$_2$}$_{1.0}$(UPy-PEB-UPy)$_{1.0}$	1937 ± 265	21 ± 5	180−200
{[Fe(Mebip-PEB-Mebip)](ClO$_4$)$_2$}$_{1.0}$(UPy-PEB-UPy)$_{0.7}$	1747 ± 383	13 ± 3	200−210
{[Fe(Mebip-PEB-Mebip)](ClO$_4$)$_2$}$_{1.0}$(UPy-PEB-UPy)$_{0.5}$	2147 ± 224	16 ± 5	200−205
{[Fe(Mebip-PEB-Mebip)](ClO$_4$)$_2$}$_{1.0}$(UPy-PEB-UPy)$_{0.3}$	1840 ± 329	20 ± 2	200−210

[a]Data represent averages from three to ten samples per film measured.

Figure 7. (A) Representative dynamic mechanical thermal analysis (DMTA) traces of films of the neat metallosupramolecular polymer [Fe(Mebip-PEB-Mebip)](ClO$_4$)$_2$ (black), the neat UPy-PEB-UPy (red), and the following blends {[Fe(Mebip-PEB-Mebip)](ClO$_4$)$_2$}$_{1.0}$(UPy-PEB-UPy)$_{1.0}$ (blue), {[Fe(Mebip-PEB-Mebip)](ClO$_4$)$_2$}$_{1.0}$(UPy-PEB-UPy)$_{0.7}$ (gray), {[Fe(Mebip-PEB-Mebip)](ClO$_4$)$_2$}$_{1.0}$(UPy-PEB-UPy)$_{0.5}$ (green), and {[Fe(Mebip-PEB-Mebip)](ClO$_4$)$_2$}$_{1.0}$(UPy-PEB-UPy)$_{0.3}$ (pink). (B) Three traces of the blend {[Fe(Mebip-PEB-Mebip)](ClO$_4$)$_2$}$_{1.0}$(UPy-PEB-UPy)$_{0.7}$ which transition around 60−75 °C.

SAXS spectra where two phases were determined to be present in the supramolecular polymer blends, thus allowing for a steplike decrease in E' when the UPy stacks melt. However, stress−strain experiments conducted at 25 °C reveal that the blends of {[Fe(Mebip-PEB-Mebip)](ClO$_4$)$_2$}$_{1.0}$(UPy-PEB-UPy)$_x$ have a slightly lower maximum stress at break (ca. 0.8−0.9 MPa) (Table S1 and Figure S11) than UPy-PEB-UPy (1.7 MPa). Additionally, the strain at break of the blends (22−31%) is similar to the [Fe(Mebip-PEB-Mebip)](ClO$_4$)$_2$ control (33%) with the exception of a high UPy content of 1.0 where the material fails at 15% strain (Table S1 and Figure S11). Taking into consideration the combined data from UV−vis titrations, SAXS, and DMTA, we conclude that the Fe-based supramolecular polymer blends are orthogonal where the Fe^{2+}-Mebip and UPy-UPy interactions likely do not recombine, and therefore, the UPy-UPy dimers can be selectively targeted using temperature as a stimulus.

Chemoresponsive Behavior. Having demonstrated the selective thermal dissociation of the UPy stacking, we sought to selectively disassemble the Fe^{2+}-Mebip motifs while leaving the UPy-UPy dimers unscathed. As iron(II) salts are known to coordinate with a variety of ligands, including multidentate amine-based molecules, we speculated that a competitive ligand for Fe^{2+} could be used to selectively disassemble the Fe-based

MSP and trigger a chemoresponse. We elected to utilize N,N,N′,N″,N″-pentanemethyldiethylenetriamine (PMDETA) as the ligand and explored if motif could be used to disassemble the MSP portion of the{[Fe(Mebip-PEB-Mebip)]-(ClO$_4$)$_2$}$_{1.0}$(UPy-PEB-UPy)$_{0.7}$ blend, which was selected because of its specific thermal transition (60 to 75 °C corresponding to the thermal dissociation of the UPy stacking) observed in DMTA (Figure 7b). A solution of {[Fe(Mebip-PEB-Mebip)](ClO$_4$)$_2$}$_{1.0}$(UPy-PEB-UPy)$_{0.7}$ in CHCl$_3$ has a characteristic deep purple color due to the MLCT transition of Fe^{2+}-Mebip complexes (Figure 8a). The addition of PMDETA (40 equiv) in solution resulted in a change of appearance within minutes from deep purple to a light brownish color due to the formation of Fe^{2+}-PMDETA complexes (Figure 8b). Analysis by UV−vis absorption spectroscopy confirms the disruption of Fe^{2+}-Mebip complexes, as the MLCT transition (λ_{max} = 565 nm) disappears completely (Figure 9). When Fe(ClO$_4$)$_2$ (85 equiv) was added to the solution with PMEDTA, the characteristic deep purple color and MLCT transition of Fe^{2+}-Mebip complexes were restored (Figure 9). Thus, these observations clearly show the switchability of the Fe^{2+}-Mebip complexes with PMDETA in solution.

The same switching scheme was applied to thin films. As a control, films of UPy-PEB-UPy were swollen in CH$_3$CN/
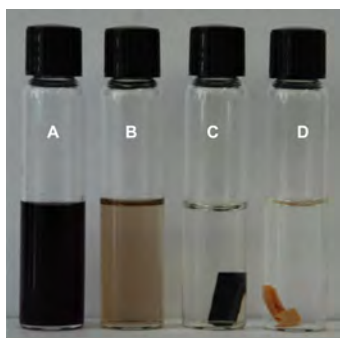
Figure 8. Photograph of (A) a solution comprising {[Fe(Mebip-PEB-Mebip)](ClO$_4$)$_2$}$_{1.0}$(UPy-PEB-UPy)$_{0.7}$ (16 μM) in CHCl$_3$ and (B) the same solution after addition of 40 equiv of PMDETA. The photograph also shows (C) a blend film of {[Fe(Mebip-PEB-Mebip)]-(ClO$_4$)$_2$}$_{1.0}$(UPy-PEB-UPy)$_{0.7}$ in CH$_3$CN and (D) the same film 30 min after the addition of 40 equiv of PMDETA to the solution.
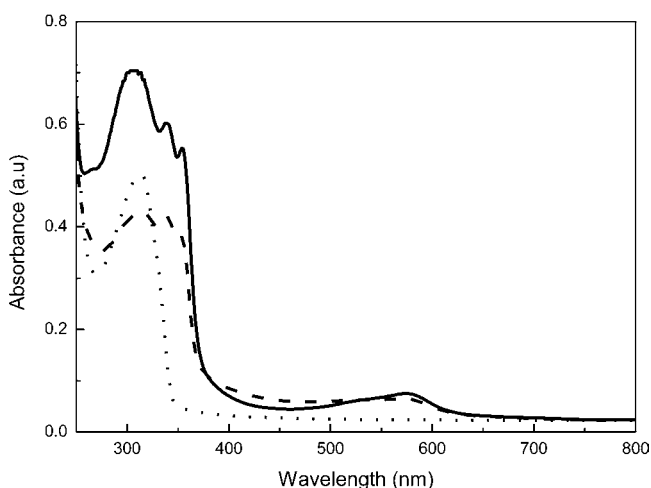
Figure 9. UV−vis absorption spectra of a solution of the blend {[Fe(Mebip-PEB-Mebip)](ClO$_4$)$_2$}$_{1.0}$(UPy-PEB-UPy)$_{0.7}$ (16 μM) in CHCl$_3$. The spectra show the original solution (—), the solution after addition of 40 equiv of PMDETA (···), and the solution after addition of 40 equiv of PMDETA and subsequently 85 equiv of Fe(ClO$_4$)$_2$ (- - -).

PMDETA (t = 30 min, 6 h, and 12 h), subsequently dried, and analyzed by DMTA. A slight increase of the storage modulus was observed in the UPy-PEB-UPy films, likely due to solvent annealing effects; however, all samples underwent a catastrophic failure at ca. 60−80 °C (Figures S7). Also, the morphology of UPy-PEB-UPy did not change in these conditions (Figure S9a). These results suggest that the introduction of PMDETA did not affect the UPy binding in UPy-PEB-UPy homopolymer films nor had it any other notable influence on the material. Films of {[Fe(Mebip-PEB-Mebip)]-(ClO$_4$)$_2$}$_{1.0}$(UPy-PEB-UPy)$_{0.7}$ were also swollen in CH$_3$CN and CH$_3$CN/PMDETA (40 equiv of PMDETA vs Mebip-PEB-Mebip). The swollen film had a weight/volume of 6 mg/mL and showed to uptake 50% of the CH$_3$CN solution after 12 h (Figure S6), and a color change was observed only after 30 min of swelling in CH$_3$CN/PMDETA. Upon longer incubation times the deep purple color of the films completely disappeared (Figure 8d). The mechanical properties of the "bleached" films were also explored by DMTA after imbibing the samples for 30 min, 6 h, and 12 h in the PMDETA solution and subsequently drying (Figure 10). After 30 min in CH$_3$CN/PMDETA, a small
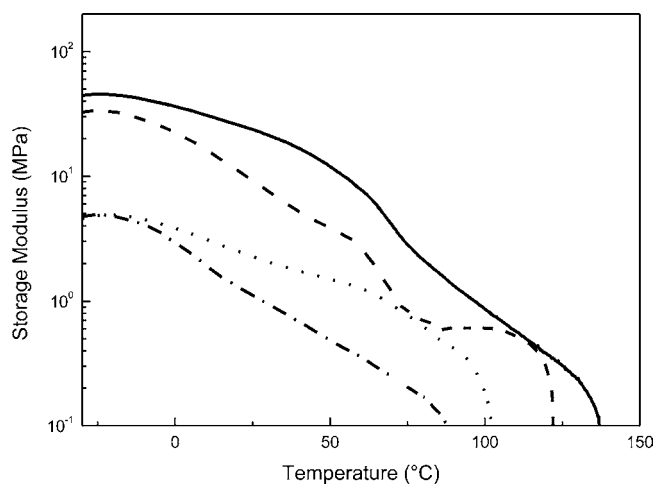
Figure 10. Representative dynamic mechanical thermal analysis (DMTA) traces of the blend films {[Fe(Mebip-PEB-Mebip)]-(ClO$_4$)$_2$}$_{1.0}$(UPy-PEB-UPy)$_{0.7}$, neat (—), with addition of 40 equiv of PMDETA (vs Mebip-PEB-Mebip) in CH$_3$CN solution and swollen for 30 min (- - -), 6 h (···), and 12 h (− · −) and annealed under vacuum for a day.

decrease is observed in the storage modulus, and after passing 60 °C, the point at which the UPy dimers melt, the storage modulus decreases severally until the sample failed at ca. 125 °C. This trend was more pronounced after imbibing the sample for 6 and 12 h, where a greater decrease in the E' was observed and the materials failed at ca. 100 and 80 °C, respectively (Figure 10). Collectively, these results demonstrate that the Fe^{2+}-Mebip interactions can be selectively disrupted by introduction of PMDETA, which, however, leaves the UPy-UPy interactions unperturbed.

■ CONCLUSIONS

In this work, we have used a synthetically straightforward approach to combine chemically orthogonal motifs by blending two types of supramolecular polymers, namely [M(Mebip-PEB-Mebip)](X)$_2$ (M = Zn, Fe; X = NTf$_2$, ClO$_4$) and UPy-PEB-UPy. The degree of orthogonal function in the supramolecular polymer blends was explored by UV−vis spectroscopy, SAXS, and DMTA. Blends of {[Zn(Mebip-PEB-Mebip)]-(NTf$_2$)$_2$}$_{1.0}$(UPy-PEB-UPy)$_x$ were determined to have a statistical mixture of interactions of Zn^{2+}-Mebip, UPy-UPy, and Zn^{2+}-UPy, and the mechanical properties of these materials were largely determined by the degree of phase-segregated lamellar morphology of a given sample.

Conversely, supramolecular polymer films based on {[Fe-(Mebip-PEB-Mebip)](ClO$_4$)$_2$}$_{1.0}$(UPy-PEB-UPy)$_x$ were shown to be both chemically and functionally orthogonal. A series of UV−vis titrations demonstrated that the Fe^{2+}-Mebip complexes can form in the presence of UPy motifs, to result in blends with Fe^{2+}-Mebip and UPy-UPy noncovalent interactions. Additionally, DMTA revealed two transitions for the melting of a hard phase where UPy-UPy dimers dissociate at relatively low temperature (ca. 60 °C) concomitant with a decrease in the storage modulus until a catastrophic failure (ca. 180 °C) due to the melting of Fe^{2+}-Mebip cross-links. Moreover, the Fe^{2+}-Mebip interactions were selectively disrupted by the addition of a competitive ligand, PMDETA, where a disappearance of the characteristic deep-purple color of Fe^{2+}-Mebip and a decrease in the failure temperature of the materials were observed.

This study highlights the complexity of orthogonal functionality with two supramolecular elastomeric polymers and the possibility to use polymer blends to create multifunctional materials that are both chemically and functionally orthogonal. This allows one to tailor new classes of "smart materials" that can respond to more than one set of well-defined stimuli to elicit more than one response.

■ ASSOCIATED CONTENT

Ⓢ Supporting Information

UV−vis spectra, SAXS data, swelling behavior, DMTA, tensile tests, and ^{1}H NMR spectra. This material is available free of charge via the Internet at http://pubs.acs.org.

■ AUTHOR INFORMATION

Corresponding Authors
*E-mail: christoph.weder@unifr.ch (C.W.).
*E-mail: gina.fiore@unifr.ch (G.L.F.).

Notes
The authors declare no competing financial interest.

■ ACKNOWLEDGMENTS

■ REFERENCES

(1) Whittell, G. R.; Manners, I. *Adv. Mater.* **2007**, *19*, 3439−3468.
(2) Fiore, G. L.; Rowan, S. J.; Weder, C. *Chem. Soc. Rev.* **2013**, *42*, 7278−7288.
(3) Jochum, F. D.; Theato, P. *Chem. Soc. Rev.* **2013**, *42*, 7468−7483.
(4) Hart, L. R.; Harries, J. L.; Greenland, B. W.; Colquhoun, H. M.; Hayes, W. *Polym. Chem.* **2013**, *4*, 4860−4870.
(5) Herbst, F.; Döhler, D.; Michael, P.; Binder, W. H. *Macromol. Rapid Commun.* **2013**, *34*, 203−220.
(6) Heinzmann, C.; Coulibaly, S.; Roulin, A.; Fiore, G. L.; Weder, C. *ACS Appl. Mater. Interfaces* **2014**, *6*, 4713−4719.
(7) Hsu, L.; Weder, C.; Rowan, S. J. *J. Mater. Chem.* **2011**, *21*, 2812−2822.
(8) Bai, S.; Zou, H.; Dietsch, H.; Simon, Y. C.; Weder, C. *Macromol. Chem. Phys.* **2014**, *215*, 398−404.
(9) Li, S.-L.; Xiao, T.; Lin, C.; Wang, L. *Chem. Soc. Rev.* **2012**, *41*, 5950−5968.
(10) Yang, S. K.; Ambade, A. V.; Weck, M. *Chem. Soc. Rev.* **2011**, *40*, 129−137.
(11) Ambade, A. V.; Yang, S. K.; Weck, M. *Angew. Chem., Int. Ed.* **2009**, *48*, 2894−2898.
(12) Nair, K. P.; Breedveld, V.; Weck, M. *Macromolecules* **2011**, *44*, 3346−3357.
(13) Mansfeld, U.; Winter, A.; Hager, M. D.; Festag, G.; Hoeppener, S.; Schubert, U. S. *Polym. Chem.* **2013**, *4*, 3177−3181.
(14) Mansfeld, U.; Winter, A.; Hager, M. D.; Hoogenboom, R.; Gunther, W.; Schubert, U. S. *Polym. Chem.* **2013**, *4*, 113−123.
(15) Mes, T.; Koenigs, M. M. E.; Scalfani, V. F.; Bailey, T. S.; Meijer, E. W.; Palmans, A. R. A. *ACS Macro Lett.* **2011**, *1*, 105−109.
(16) Balkenende, D. W. R.; Coulibaly, S.; Balog, S.; Simon, Y. C.; Fiore, G. L.; Weder, C. *J. Am. Chem. Soc.* **2014**, *136*, 10493−10498.
(17) Burnworth, M.; Tang, L.; Kumpfer, J. R.; Duncan, A. J.; Beyer, F. L.; Fiore, G. L.; Rowan, S. J.; Weder, C. *Nature* **2011**, *472*, 334−337.
(18) Coulibaly, S.; Roulin, A.; Balog, S.; Biyani, M. V.; Foster, E. J.; Rowan, S. J.; Fiore, G. L.; Weder, C. *Macromolecules* **2013**, *47*, 152−160.
(19) Biyani, M. V.; Foster, E. J.; Weder, C. *ACS Macro Lett.* **2013**, *2*, 236−240.
(20) Gohy, J.-F.; Lohmeijer, B. G. G.; Décamps, B.; Leroy, E.; Boileau, S.; van den Broek, J. A.; Schubert, D.; Haase, W.; Schubert, U. S. *Polym. Int.* **2003**, *52*, 1611−1618.
(21) Montero de Espinosa, L.; Balog, S.; Weder, C. *ACS Macro Lett.* **2014**, *3*, 540−543.
(22) Weng, W.; Li, Z.; Jamieson, A. M.; Rowan, S. J. *Macromolecules* **2008**, *42*, 236−246.
(23) Folmer, B. J. B.; Sijbesma, R. P.; Versteegen, R. M.; van der Rijt, J. A. J.; Meijer, E. W. *Adv. Mater.* **2000**, *12*, 874−878.
(24) Pangborn, A. B.; Giardello, M. A.; Grubbs, R. H.; Rosen, R. K.; Timmers, F. J. *Organometallics* **1996**, *15*, 1518−1520.
(25) Beijer, F. H.; Sijbesma, R. P.; Kooijman, H.; Spek, A. L.; Meijer, E. W. *J. Am. Chem. Soc.* **1998**, *120*, 6761−6769.
(26) Sijbesma, R. P.; Beijer, F. H.; Brunsveld, L.; Folmer, B. J. B.; Hirschberg, J. H. K. K.; Lange, R. F. M.; Lowe, J. K. L.; Meijer, E. W. *Science* **1997**, *278*, 1601−1604.
(27) Constable, E. C. In *Advances in Inorganic Chemistry*; Eméléus, H. J., Ed.; Academic Press: New York, 1986; Vol. 30, pp 69−121.
(28) Hofmeier, H.; Hoogenboom, R.; Wouters, M. E. L.; Schubert, U. S. *J. Am. Chem. Soc.* **2005**, *127*, 2913−2921.
(29) Holyer, R. H.; Hubbard, C. D.; Kettle, S. F. A.; Wilkins, R. G. *Inorg. Chem.* **1966**, *5*, 622−625.
(30) Appel, W. P. J.; Portale, G.; Wisse, E.; Dankers, P. Y. W.; Meijer, E. W. *Macromolecules* **2011**, *44*, 6776−6784.
(31) de Greef, T. F. A.; Nieuwenhuizen, M. M. L.; Sijbesma, R. P.; Meijer, E. W. *J. Org. Chem.* **2010**, *75*, 598−610.
(32) Kumpfer, J. R.; Wie, J. J.; Swanson, J. P.; Beyer, F. L.; Mackay, M. E.; Rowan, S. J. *Macromolecules* **2011**, *45*, 473−480.
(33) Kautz, H.; van Beek, D. J. M.; Sijbesma, R. P.; Meijer, E. W. *Macromolecules* **2006**, *39*, 4265−4267.